Dynamical Origin of Independent Spiking and Bursting Activity in Neural Microcircuits

Thomas Nowotny*
University of Sussex, Falmer, Brighton BN1 9QJ, United Kingdom

Mikhail I. Rabinovich†
Institute for Nonlinear Science, University of California San Diego, 9500 Gilman Drive, La Jolla, California 92093-0402, USA

(Received 14 September 2006; published 22 March 2007)

The relationship between spiking and bursting dynamics is a key question in neuroscience, particularly in understanding the origins of different neural coding strategies and the mechanisms of motor command generation and neural circuit coordination. Experiments indicate that spiking and bursting dynamics can be independent. We hypothesize that different mechanisms for spike and burst generation, intrinsic neuron dynamics for spiking and a modulational network instability for bursting, are the origin of this independence. We tested the hypothesis in a detailed dynamical analysis of a minimal inhibitory neural microcircuit (motif) of three reciprocally connected Hodgkin-Huxley neurons. We reduced this high-dimensional dynamical system to a rate model and showed that both systems have identical bifurcations from tonic spiking to burst generation, which, therefore, does not depend on the details of spiking activity.

DOI: 10.1103/PhysRevLett.98.128106 PACS numbers: 87.18.Sn, 05.45.−a, 82.40.Bj, 87.18.Bb

The appearance and timing relationship of oscillatory activities with strongly different frequencies in complex nonlinear systems is one of the key problems of nonlinear dynamics. Burst generation in lasers [1], mode competition in gyrotrons [2], and time-modulated oscillatory convection [3] are just a few examples illustrating the generality of this problem. In neuroscience, many experiments indicate that spiking and bursting dynamics are involved in different ways in neuronal microcircuit functions [4]. In particular, spiking (temporal) and bursting (rate) activity can be independent and code for different entities or sensory variables [5]. What is the dynamical origin of this independence? We showed here that over a large dynamical range the bursting dynamics does not depend on exact spike timing or detailed spiking activity if it results from the network interaction of spiking neurons. We are particularly interested in the class of dynamical systems that describe typical motifs (building blocks) of complex neural circuits, the most common one a circuit of three coupled inhibitory neurons [6]. For the first time we have observed a sequence of bifurcations that leads to the appearance of a heteroclinic cycle [7] in the high-dimensional phase space of a system built of elements with complex intrinsic dynamics. This heteroclinic cycle consists of saddle limit cycles (reflecting the spiking activity of neurons) and heteroclinic orbits that connect them cyclically. The heteroclinic structure is robust against finite changes of control parameters.

We compared the bifurcation sequence from tonic activity to burst generation in a network of Hodgkin-Huxley (HH) spiking neurons with the sequence of bifurcations that leads to the appearance of a heteroclinic cycle in the framework of a time-averaged (rate) model of the same network. We found that these sequences are the same.

The motif network consists of three HH neurons reciprocally connected by inhibitory synapses. The neurons are described by standard HH equations,

$$C\frac{dV_i(t)}{dt} = -I_{\mathrm{Na}} - I_{\mathrm{K}} - I_{\mathrm{leak}} - I_{\mathrm{syn}} - I_{\mathrm{stim}}, \qquad (1)$$

where $i = 1, 2, 3$ denotes the number of the neuron, the leak current is given by $I_{\mathrm{leak}}(t) = g_{\mathrm{leak}}[V_i(t) - E_{\mathrm{leak}}]$, and $I_{\mathrm{Na}}(t)$ and $I_{\mathrm{K}}(t)$ were [8]

$$\begin{aligned} I_{\mathrm{Na}}(t) &= g_{\mathrm{Na}} m_i(t)^3 h_i(t)[V_i(t) - E_{\mathrm{Na}}], \\ I_{\mathrm{K}}(t) &= g_{\mathrm{K}} n_i(t)^4 [V_i(t) - E_{\mathrm{K}}]. \end{aligned} \qquad (2)$$

I_{stim} is a constant input current to each neuron making it tonically spiking with I_{stim}-dependent frequency. Each activation and inactivation variable $y_i(t) = \{n_i(t), m_i(t), h_i(t)\}$ satisfied first-order kinetics

$$\frac{dy_i(t)}{dt} = \alpha_y(V_i(t))[1 - y_i(t))] - \beta_y(V_i(t))y_i(t), \qquad (3)$$

with nonlinear functions $\alpha_y(V)$ and $\beta_y(V)$ given by

$$\begin{aligned} \alpha_n &= 0.032(-50 - V)/\{\exp[(-5 - V)/5] - 1\}, \\ \beta_n &= 0.5\exp[(-55 - V)/40], \\ \alpha_m &= 0.32(-52 - V)/\{\exp[(-52 - V)/4] - 1\}, \\ \beta_m &= 0.28(25 + V)/\{\exp[(25 + V)/5] - 1\}, \\ \alpha_h &= 0.128\exp[(-48 - V)/18], \\ \beta_h &= 4/\{\exp[(-25 - V)/5] + 1\}. \end{aligned} \qquad (4)$$

The parameter values were $C = 0.03\ \mu$F, $g_{\mathrm{leak}} = 1\ \mu$S, $E_{\mathrm{leak}} = -64$ mV, $g_{\mathrm{Na}} = 360\ \mu$S, $E_{\mathrm{Na}} = 50$ mV, $g_{\mathrm{K}} = 70\ \mu$S, $E_{\mathrm{K}} = -95$ mV.

The synaptic current onto neuron j is the linear sum of the currents of all incoming synapses, $I_{\text{syn},j} = \sum_i I_{\text{syn},ji}$ where the individual currents are (modified from [9])

$$I_{\text{syn},ji} = g_{ji} S_i (V_j - V_{\text{rev}}), \tag{5}$$

$$\tau \frac{dS_i}{dt} = (R_i - \kappa S_i) \frac{S_{\max} - S_i}{S_{\max}}, \tag{6}$$

$$\tau \frac{dR_i}{dt} = \Theta(V_i - V_{\text{th}}) - R_i, \tag{7}$$

where the threshold potential for transmitter release was $V_{\text{th}} = -20$ mV, the synaptic time scale $\tau = 50$ ms, the maximal fraction of postsynaptically bound transmitter $S_{\max} = 0.045$, the relative rate of transmitter binding and unbinding $\kappa = 1/2$, and Θ denotes the Heaviside step function. R_i is a measure of the amount of neurotransmitter released presynaptically and S_i the fraction of postsynaptically bound neurotransmitter. In the following all indices are cyclical. For visualization and analysis of bursting dynamics we use S_i, which is essentially a low-pass filtered version of the spikes in the membrane potential V_i of the presynaptic neuron.

Reduction to a rate model.—The presynaptic release of transmitter R_i is driven by spikes, each spike contributing just a little to the total value of R_i, such that we can approximate the resulting average release r_i of the presynaptic spike train by a rate equation [compare to (7)] $\tau \frac{dr_i}{dt} = a(x_i) - r_i$, where a is an unspecified function of x_i, the rate of spiking of the neuron i. We determine the function a by requiring that $r_i = R_i$ for a tonic presynaptic spike train, leading to

$$\tau \frac{dr_i}{dt} = \frac{1 - \exp(-\tau_{\text{spike}}/\tau)}{1 - \exp[-1/(x_i \tau)]} - r_i, \tag{8}$$

where τ_{spike} is the spike width measured at $V_i = 0$ mV, in our case $\tau_{\text{spike}} = 0.695$ ms. Except during a spike, V_i is approximately constant, such that we can substitute V_{rest} for it (denoting the approximated S_i by s_i):

$$I_{\text{syn},j} = -\sum_i g_{ji} s_i (V_{\text{rest}} - V_{\text{rev}}) = -\sum_i \hat{g}_{ji} s_i, \tag{9}$$

where the constant voltage difference was absorbed into $\hat{g}_{ji}$. Furthermore, the HH neuron model has a very clear relationship of spike rate to input current, which can be approximated excellently by

$$x_i = x_0 [\max\{(I_{\text{syn},i} + I_{\text{dc}} - I_0)/\text{nA}, 0\}]^{\alpha}, \tag{10}$$

with $I_0 = 0.0439$ nA, $\alpha = 0.564$, and $x_0 = 0.185$, a least squares fit (Fig. 1), which is more precise than using linear f-I curves [10] and leads to quantitative agreement of rate and spiking model (see below).

Denoting $\tilde{g}_{ij} = \hat{g}_{ij}/\text{nA}$, $\tilde{I} = (I_{\text{dc}} - I_0)/\text{nA}$, we obtain

$$x_i = x_0 \left[\tilde{I} - \sum_j \tilde{g}_{ij} s_j \right]_+^{\alpha}, \tag{11}$$

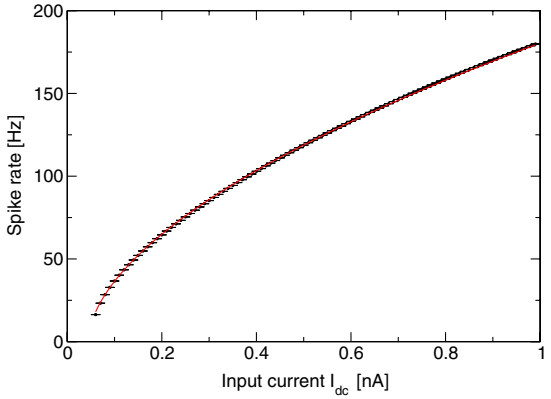

FIG. 1 (color online). Rate response x of the HH neuron model (1)–(4) to dc input currents I_{dc} (bullets). It is fitted almost perfectly by (10) (thin line).

with $[\ldots]_+^{\alpha} \equiv (\max\{\ldots, 0\})^{\alpha}$. Inserting (11) into (8) yields

$$\tau \frac{dr_i}{dt} = \frac{1 - \exp(-\tau_{\text{spike}}/\tau)}{1 - \exp\{-(x_0 [\tilde{I} - \sum_j \tilde{g}_{ij} s_j]_+^{\alpha} \tau)^{-1}\}} - r_i$$

$$\approx \tilde{x}_0 \left[\tilde{I} - \sum_j \tilde{g}_{ij} s_j \right]_+^{\alpha} \tau - r_i, \tag{12}$$

where we used $\exp(x) \approx 1 + x$ for small $|x|$, and $\tilde{x}_0 = [1 - \exp(-\tau_{\text{spike}}/\tau)] x_0$. We, thus, arrive at an approximate rate model of the form

$$\tau \frac{ds_i}{dt} = (r_i - \kappa s_i) \frac{S_{\max} - s_i}{S_{\max}}, \tag{13}$$

$$\tau \frac{dr_i}{dt} = \tilde{x}_0 \left[\tilde{I} - \sum_j \tilde{g}_{ij} s_j \right]_+^{\alpha} \tau - r_i, \tag{14}$$

where $\tilde{x}_0 \approx 2.57 \times 10^{-3}$, $\tilde{I} \approx I_{\text{dc}}/\text{nA} - 0.0439$, $\tilde{g}_{ij} \approx 20 g_{ij}$ mV/nA, and (13) is the equivalent of (6).

Multistability.—The behavior of the dynamical system (1)–(7) strongly depends on the level of symmetry of the connections among the oscillatory elements of the network (the autonomous activity of each neuron is a stable limit cycle of tonic spiking). If the system is close to being symmetrical ($g_{ij} \approx g_{ji}$) the bifurcations in the system (1)–(7) shown in Figs. 2(a)–2(d) and the ensuing transformations of the phase portrait depend only on one control parameter, i.e., the equal strength of the couplings $g_{ij} = g_{ji} = g$. For weak competition, all neurons are in a tonic spiking regime [3D torus or a limit cycle on it in case of spike synchronization in the original phase space, and a stable node in the $\mathcal{S} = (S_1, S_2, S_3)$ space [Fig. 2(a)]]; the limit sets corresponding to a single or a pair of active neurons do not exist. For stronger competition, the system demonstrates multistability, i.e., the stable 3D torus or limit cycle coexists with three stable 2D tori (or limit cycles in case of spike synchronization) corresponding to simultaneous spiking dynamics of different pairs of two neurons.

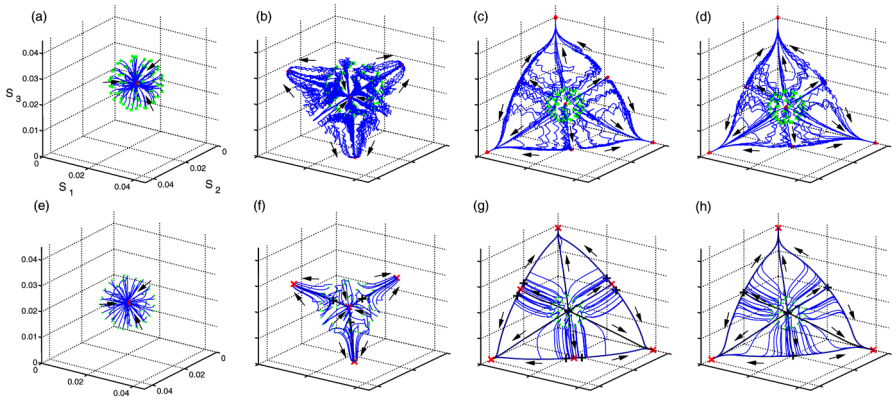

FIG. 2 (color online). Bifurcations of the 3 neuron HH circuit (a)–(d) in comparison to the rate model (e)–(h) for symmetric reciprocal interaction of increasing strength. The three displayed variables are the synaptic activation $\mathcal{S}$ of the synapses originating from each of the three neurons, respectively. This quantity is a low-pass filtered version of the neuron's spike train in case of the spiking neurons and thus provides a ''rate description'' of the spiking activity. The bifurcations are identical in both cases and even the exact critical values of g are very close. Synaptic conductances (a) $g = 10$ nS, (b) $g = 30$ nS, (c) $g = 50$ nS, (d) $g = 60$ nS, (e) $g = 30$ nS, (f) $g = 40$ nS, (g) $g = 51.4$ nS, (h) $g = 60$ nS. $\times$ denotes nodes and + saddle points.

In the $\mathcal{S}$ phase space, the boundaries of the basins of attraction of these attractors are separatrices of saddles. When the competition increases further [Fig. 2(c)] these saddles that are close to the symmetric attractor merge with this stable node (in $\mathcal{S}$ space), which after bifurcation becomes a saddle itself. The observed phenomena are identical to the bifurcations present in the 3-neuron approximate rate model (13) and (14) shown in Figs. 2(e)–2(h), for which we know the exact location of all fixed points and the bifurcations (Fig. 3).

Heteroclinic structure.—To understand the mechanism of burst generation, we have to analyze the bifurcations occurring for increasingly asymmetric connections between neurons. We denote the conductance of synapses in one direction by g_1 and in the opposite direction by g_2 and change their relative strength. The corresponding sequence of bifurcations in the $\mathcal{S}$ space is shown in Fig. 2(c), 4(a), and 4(b). For increasing asymmetry the saddles in the $\mathcal{S}$ space are moving closer to the stable nodes that correspond to three different tonic spiking modes (one tonic and

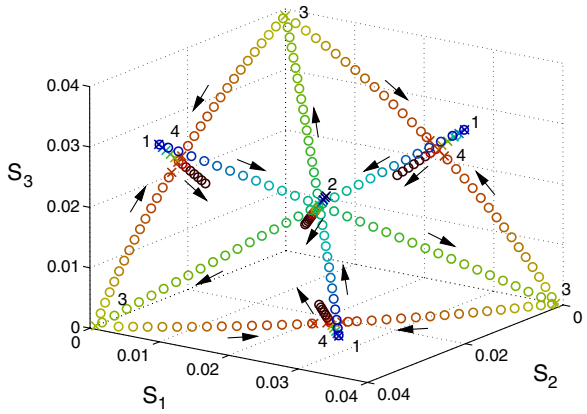

FIG. 3 (color online). Bifurcations of the symmetric rate model (obtained with AUTO-07p [14]). Nodes are crosses and saddle points circles. The control parameter g is color coded, and increasing g moves fixed points along the arrows. The bifurcations are (for increasing g) (a) three nodes and three saddles appear at 1 ($g = 35.1$ nS), (b) the middle node merges with the saddles coming from 1, becomes a saddle, and three new saddles appear that move towards 3 ($g = 41.58$ nS), (c) the three saddles reach 3, become nodes, and give rise to a pair of saddles each ($g = 46.3$ nS), and (d) the saddles merge with the three fixed points at 4, form three new saddles, and the nodes at 3 remain the only stable fixed points ($g = 51.5$ nS).

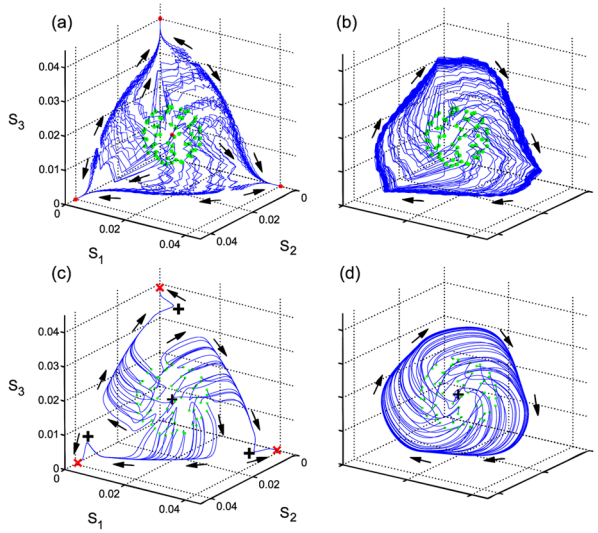

FIG. 4 (color online). Bifurcation of the HH model (a),(b) for increasing asymmetry of the connections compared to the same transition in the rate model (c),(d). We, again, find the same structure: The saddle points move to the corners and eventually merge with the fixed points, vanish, and give rise to a globally attracting limit cycle of bursting dynamics. (a) $g_1 = 60$ nS, $g_2 = 45$ nS, (b) $g_1 = 80$ nS, $g_2 = 35$ nS, (c) $g_1 = 60$ nS, $g_2 = 50$ nS, and (d) $g_1 = 80$ nS, $g_2 = 35$ nS.

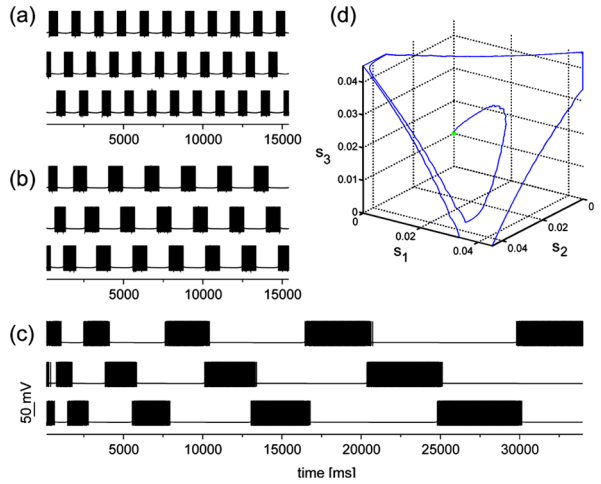

FIG. 5 (color online). (a)–(c) Time series of the membrane potentials V_i of the three neurons. (a) $I_{\mathrm{stim}} = 0.08$ nA, (b) $I_{\mathrm{stim}} = 0.16$ nA, and (c) $I_{\mathrm{stim}} = 0.22$ nA. The higher the intrinsic spiking rate of the neuron (determined by I_{stim}), the closer comes the limit cycle to the heteroclinic cycle. For (c) the heteroclinic cycle is attracting and the time series of bursts continues to slow down infinitely. (d) Rate ($\mathcal{S}$ space) picture of the dynamics in (c), approaching the heteroclinic cycle.

two silent neurons). At a critical value of the ratio g_1/g_2, the saddles merge with the stable nodes, which become saddles themselves, leading to the appearance of a heteroclinic cycle [Fig. 3(c) and 3(d)]. The corresponding bifurcations in the phase space of the rate model (13) and (14) coincide with the observed bifurcations in the complete, complex system (1)–(7), like in the symmetric case. Thus, the bursting dynamics does not depend on the details of spike timing.

Stable heteroclinic sequence.—For high intrinsic spiking frequency of the constituent neurons the synapses are driven towards saturation which slows down their intrinsic dynamics which, in turn, reduces the bursting frequency of the circuit (Fig. 5). For sufficiently large intrinsic spiking frequency of the neurons, the heteroclinic cycle becomes *attracting* [11]: The bursting dynamics slows down indefinitely [Fig. 5(c)].

Conclusion.—We found the origin of burst generation in a motif circuit of three HH neurons which are reciprocally coupled with inhibitory synapses. It is a modulation instability that leads to the appearance of a heteroclinic sequence in the high-dimensional phase space of the corresponding dynamical system (see its projection to $\mathcal{S}$ space in Fig. 4(a) and 4(b)]. Based on the similarity of the bifurcations towards heteroclinic sequences in the original complex system and in the time-averaged rate model we introduced, one can conclude that bursting dynamics does not depend on the details of neuronal spiking activity of individual neurons. The dynamical image of rhythmic bursting activity in $\mathcal{S}$ space is a stable limit cycle in the vicinity of a heteroclinic sequence [12]. In addition, we confirmed the validity of the time-averaged rate model for the description of network bursting dynamics.

While we chose to investigate a minimal motif of three neurons in this work, the phenomena of switching activity between quasistationary states typical for a heteroclinic structure have been observed *in vivo* in the much larger cortex network (Fig. 2 in [13]).

We thank Valentin Afraimovich for many helpful discussions. This work was supported by the NSF, Grants No. PHY-0414174 and No. EIA-0130708, and the NSF/NIH, Grant No. RO1 NS050945.

*Electronic address: T.Nowotny@sussex.ac.uk
†Electronic address: mrabinovich@ucsd.edu

[1] R. Meucci, A. Di Garbo, E. Allaria, and F. T. Arecchi, Phys. Rev. Lett. **88**, 144101 (2002).
[2] G. P. Saraph, T. M. Antonsen, Jr., G. S. Nusinovich, and B. Levush, Phys. Plasmas **2**, 2839 (1995).
[3] H. Riecke, J. D. Crawford, and E. Knobloch, Phys. Rev. Lett. **61**, 1942 (1988).
[4] N. Masuda, Neural Comput. **18**, 45 (2006); E. Schneidman, W. Bialek, and M. J. Berry II, J. Neurosci. **23**, 11 539 (2003).
[5] J. Huxter, N. Burgess, and J. O'Keefe, Nature (London) **425**, 828 (2003).
[6] O. Sporns and R. Kotter, PLOS Biology **2**, e369 (2004).
[7] F. Busse and K. Heikes, Science **208**, 173 (1980); J. Guckenheimer and P. Holmes, Math. Proc. Cambridge Philos. Soc. **103**, 189 (1988); G. Saari, *The Basic Geometry of Voting* (Springer, Berlin, 1995); M. Rabinovich, A. Volkovskii, P. Lecanda, R. Huerta, H. D. I. Abarbanel, and G. Laurent, Phys. Rev. Lett. **87**, 068102 (2001); M. I. Rabinovich, P. Varona, A. I. Selverston, and H. D. I. Abarbanel, Rev. Mod. Phys. **78**, 1213 (2006).
[8] R. D. Traub and R. Miles, *Neural Networks of the Hippocampus* (Cambridge University Press, New York, 1991).
[9] W. Rall, J. Neurophysiol. **30**, 1138 (1967).
[10] O. Shriki, D. Hansel, and H. Sompolinsky, Neural Comput. **15**, 1809 (2003).
[11] A stable (attracting) heteroclinic cycle attracts all trajectories in its vicinity, i.e., it behaves like a stable limit cycle (with infinite period).
[12] The image of rhythmic spiking-bursting activity in the phase space of the system (1)–(7) is an attracting 2D torus with unclosed winding in the general case or closed winding in the case of high order synchronization between spiking and bursting oscillations.
[13] M. Abeles, H. Bergman, I. Gat, I. Meilijson, E. Seidmann, and N. Tishby, Proc. Natl. Acad. Sci. U.S.A. **92**, 8616 (1995).
[14] E. J. Doedel, http://indy.cs.concordia.ca/auto/.